frontiers | Frontiers in Earth Science

TYPE Original Research
PUBLISHED 20 October 2025
DOI 10.3389/feart.2025.1636508

OPEN ACCESS

EDITED BY
Dicky Harishidayat,
Pertamina Hulu Energi, Indonesia

REVIEWED BY
Harya Dwi Nugraha,
University of Bergen, Norway
John Oluwadamilola Olutoki,
Queensland University of Technology Faculty of Science, Australia

*CORRESPONDENCE
Yinglin Zhang,
zyl18611799663@163.com

RECEIVED 28 May 2025
ACCEPTED 29 September 2025
PUBLISHED 20 October 2025

CITATION
Zhang Y, Sun H, Xu L, Yan H, Wang X and Chen B (2025) Reservoir potential of the Eocene deltaic lacustrine system in the Pearl River Mouth Basin.
Front. Earth Sci. 13:1636508.
doi: 10.3389/feart.2025.1636508

Reservoir potential of the Eocene deltaic lacustrine system in the Pearl River Mouth Basin

Yinglin Zhang[1,2]*, Hui Sun[1,2], Leyi Xu[1,2], Hui Yan[1,2], Xiaomeng Wang[1,2] and Beichen Chen[1,2]

[1]Shenzhen Branch of China National Offshore Oil Corporation (CNOOC) Co., Ltd., Shenzhen, China, [2]CNOOC Deepwater Development, Shenzhen, China

With ongoing exploration and development in the Baiyun Sag, its southwestern portion has emerged as a promising target for significant hydrocarbon discoveries. However, commercial discoveries have yet to be achieved due to limited reservoir areal extent and tight reservoir properties. To resolve reservoir architecture and quality, we integrate seismic and core data, building a depositional-diagenetic model of the Eocene Enping Formation in the block L13. The results show that the Enping braid deltas, sourced from the Shunhe Uplift, contain HST delta-front channels that constitute the principal reservoirs. Reservoirs comprise feldspathic litharenite and litharenite, with moderate-low porosity (6.6–21.1%) and low-ultralow permeability (0.02–21.30 mD). Pore systems are typified by tuffaceous dissolution pores and feldspar dissolution pores, with reservoir quality governed by the interplay of depositional and diagenetic processes. Coarser-grained textures in delta-front subaqueous distributary channels provide favorable reservoir frameworks, whereas compaction dominates porosity-permeability reduction. The key factor in enhancing reservoir properties is the formation of intergranular dissolution pores, which arise from the dissolution of tuffaceous material and feldspar by CO_2-organic acid fluids generated during source rock evolution. This work establishes a depositional-diagenetic framework for reservoir prediction in the Enping Formation, offering critical insights for unlocking tight gas potential in the underexplored southwestern Baiyun Sag.

KEYWORDS

Baiyun sag, Enping Formation, sequence stratigraphy, delta, reservoir potential, seismic sedimentology

1 Introduction

Seismic sedimentology is an interdisciplinary field that bridges geology and geophysics. Building upon the foundations of seismic and sequence stratigraphy, its emergence and evolution since the 1970s have been driven by the invention and widespread application of 3D seismic technology. Dahm and Graebner (1979) pioneered the identification of paleogeomorphic features from meandering fluvial channels on seismic amplitude time slices. This capability prompted geophysical software companies (e.g., Landmark and GeoQuest) to develop horizon-slicing tools, which were rapidly and widely adopted across the petroleum industry. Building on this foundation, Hongliu Zeng (University of Texas at Austin) proposed the concept and generation method

of stratal slices in his PhD dissertation. Subsequently, in a series of seminal articles in Geophysics, he formally established seismic sedimentology as the discipline that integrates seismic lithology and seismic geomorphology to investigate sedimentary lithology, depositional processes, systems, and basin-fill history (Zeng et al., 1998a; Zeng et al., 1998b).

In summary, seismic sedimentology is an established interdisciplinary field grounded in modern sedimentology, sequence stratigraphy, and geophysics. It leverages 3D seismic data, integrated with core, well-log, and outcrop data, synthesizing techniques from seismic geomorphology, seismic lithology, and sequence stratigraphy. This integrated approach aims to characterize macro-scale sedimentary features, reconstruct depositional-system evolution, predict the origin and distribution of thin-bedded sand bodies, and assess reservoir quality and hydrocarbon potential.

In recent years, seismic sedimentology has gained relatively widespread application in China (Dong et al., 2006; Zhang et al., 2007; Wang et al., 2008). Particularly in offshore hydrocarbon exploration, where drilling data are limited due to high costs and operational difficulties, seismic sedimentology—with its solid theoretical basis in geology and geophysics and advanced technical methodologies—has attracted significant attention and become a focus of research within both geological and geophysical communities.

The Baiyun Sag is the primary gas exploration and production hub in the Pearl River Mouth Basin (Gao et al., 2024a). Since the commencement of large-scale independent exploration in 2000, multiple gas field groups have been discovered, including the Panyu Low Uplift Gas Field Group, Liwan-3 Gas Field Group, and Liuhua-28 Gas Field Group. These groups are predominantly distributed in the northern and eastern regions of the Baiyun Sag, with over 75% of the proven natural gas reserves concentrated within the Zhujiang Formation. As production from gas fields continues and exploration intensifies in the major producing formations, the urgency for the reserve replacement has become critical. The escalating difficulty in discovering new reserves demands exploration of new geographic areas and stratigraphic systems. The southwestern Baiyun Sag exhibits both limited prior hydrocarbon exploration activity and relatively underdeveloped research foundations regarding its petroleum geological conditions.

Tectonic activity within the study area creates favorable conditions for the fault-block structural traps. Multi-period braid delta systems are extensively developed, while sublacustrine fan systems are also occur within the lacustrine basin. The Sand-rich Strata exhibit close spatial coupling with the deep-seated fault systems, which act as highly effective hydrocarbon migration pathways. These characteristics collectively establish the southwestern Baiyun Sag as a highly prospective zone for hydrocarbon exploration (Shi et al., 2010; Mi et al., 2016).

The southwestern Baiyun Sag extends from the Yunkai Low Uplift to its southern margin (Figure 1), covering an exploration area of approximately 5,500 km^2. As of the end of 2024, only 12 exploration wells have been drilled in this region, indicating an extremely low degree of exploration and significant untapped potential. Previous studies on the Enping Formation in the Baiyun Sag have focused on structural-sedimentary responses and hydrocarbon source rock development conditions (Mi et al., 2018; Zhu et al., 2012; Ma et al., 2016). Research efforts have been concentrated in the sag's northern and eastern sectors, where exploration discoveries have already been established (Mi et al., 2006; Chen et al., 2009; Wen et al., 2022; Liao et al., 2022). In contrast, studies on reservoirs in the southwestern Baiyun Sag have centered on the Zhuhai Formation and buried hill reservoir conditions (Zhang et al., 2024; Liu et al., 2025), while research targeting the sedimentation and reservoir characteristics of the Enping Formation in this region remains limited. To address this knowledge gap, this study integrates seismic and drilling data, applying methodologies including seismic facies analysis, sedimentary facies interpretation, sequence stratigraphy, and petrological analysis to systematically investigate the reservoir development characteristics and controlling factors of the Enping Formation. The findings aim to provide critical geological insights for exploration targeting new plays and intervals within the Baiyun Sag.

2 Geological setting

The Baiyun Sag is situated in the northeastern Zhu II Depression of the Pearl River Mouth Basin. It is bordered by the Yunkai Low Uplift to the west, the Dongsha Uplift to the east, the Panyu Low Uplift to the north, and the Yunli Low Uplift to the south (Figure 1). This Cenozoic sag, initiated in the Paleogene, features a maximum sedimentary thickness exceeding 11,000 m, and covers an area of approximately 12,000 km^2, lying in present-day water depths of 200–2,000 m (Pang et al., 2008). The Baiyun Sag has undergone three distinct tectonic evolutionary stages: the Paleogene rifting phase, the Early to Middle Miocene thermal subsidence phase, and the neo-tectonic phase since the Late Miocene (Zhang et al., 2014; Zhang, 2010).

During the rifting phase, the basin experienced continuous subsidence, continuous subsidence of the basin led to the development of lacustrine sedimentary systems, including fan deltas and braid deltas, with subsequent deposition of the Eocene Wenchang, Enping, and Zhuhai formations (Li et al., 2014). During the thermal subsidence phase, intense subsidence driven by deep mantle processes occurred alongside the rapid northward migration of the shelf-slope break, this transition gradually transformed the Baiyun Sag into a deep-water slope environment, characterized by shelf-margin delta–deep-water fan depositional systems that formed the Early to Middle Miocene Zhujiang and Hanjiang formations (Liu et al., 2011a; Liu et al., 2011b). During the neo-tectonic phase, the sag underwent differential subsidence dominated by the reactivation of early faults and rapid subsidence in the central depression, this period saw the development of upper bathyal to abyssal sediments, including the Yuehai formation, Wanshan formation, and Quaternary system (He et al., 2019), this period represents the critical phase of hydrocarbon accumulation in most areas. Fault activity serves as a preferential migration pathway for deep fluids, driving secondary migration of hydrocarbons to shallow strata, and this process concurrently promotes fracture propagation and dissolution-induced porosity enhancement in tight reservoirs. The tectono-sedimentary evolution of the southwestern Baiyun Sag during the Eocene can be divided into three phases: Initial isostatic extension, Detachment rifting, and Rift-sag (Pang et al., 2018; Dong et al., 2009; Ding et al., 2009). These phases correspond to the depositional periods of the Lower Wenchang Formation

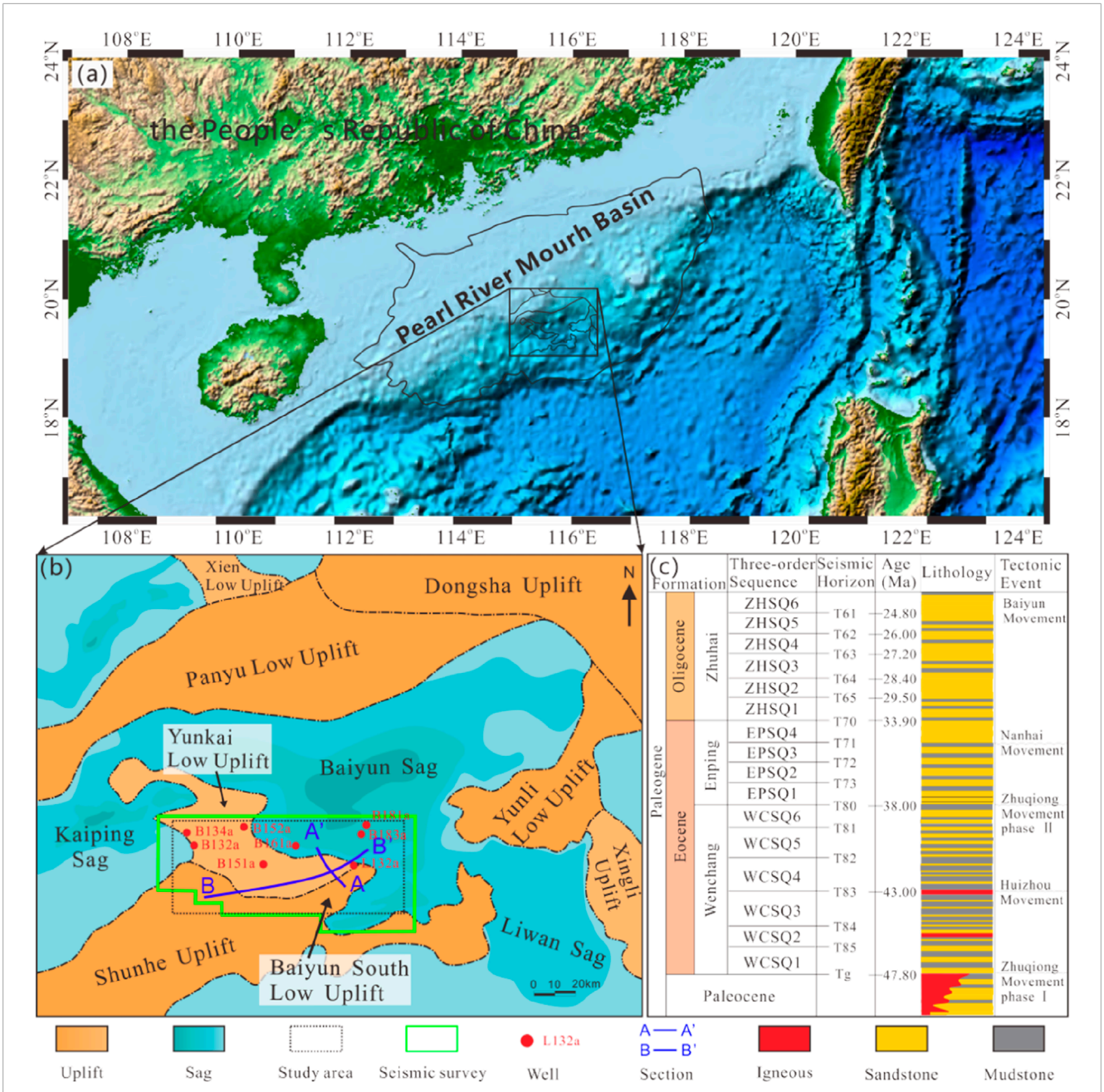

FIGURE 1
Location of block L13 and Composite stratigraphic Column of the Baiyun sag. **(a)** Regional location of Baiyun Sag; **(b)** Study area extent; **(c)** Stratigraphic column.

(deposited at ~47.8 Ma), Upper Wenchang Formation (deposited at ~38.0 Ma), and Enping Formation (deposited during 38.0–33.9 Ma).

2.1 Initial isostatic extension phase

Sedimentation in the Baiyun Sag was dominated by axial sediment supply, and multiple sub-depressions and depositional centers formed within the basin (Xie et al., 2023). The Shunhe Uplift and Yunkai Low Uplift provided the primary sediment sources for the southwestern Baiyun Sag, promoting the development of a large-scale transfer-zone delta.

2.2 Detachment rifting phase

This period featured upper crustal decoupling and lower crustal ductile extension. Under extensional detachment faulting, the Baiyun Sag underwent intense subsidence, causing expansion and integration of the early lacustrine basin into a unified large-scale deep-water lake. Concurrently, a low-gradient braid delta developed in the northern Baiyun Sag (Liu et al., 2022). And a depressional trough formed between the Shunhe Uplift and the Yunkai Low Uplift. Detrital material sourced from the Shunhe Uplift, which was obstructed by the Yunkai Low Uplift, migrated along the trough to the southwestern Baiyun Sag, forming small-scale deltas.

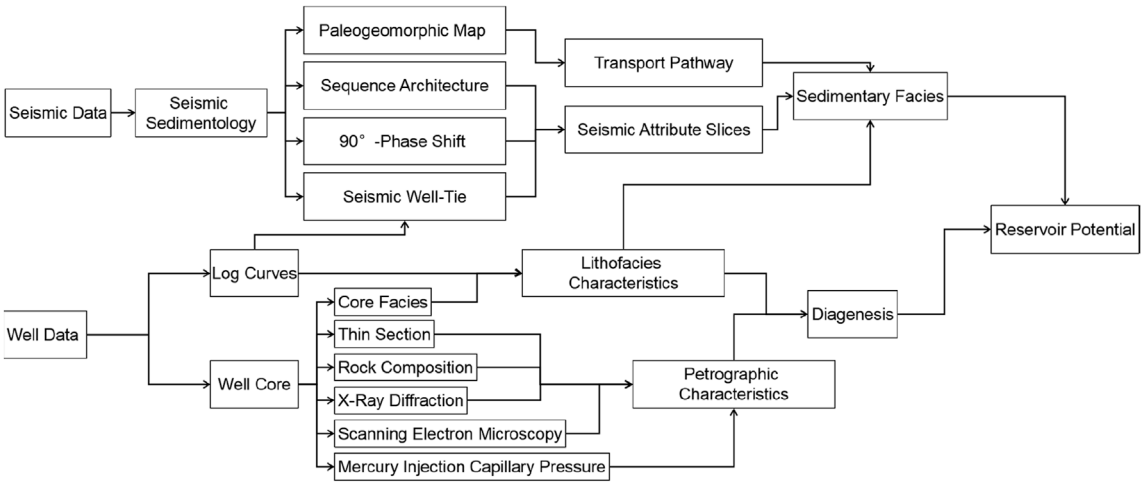

FIGURE 2
Workflow.

2.3 Rift-sag phase

Continuous lower crustal extension and thinning drove the predominant thermal subsidence in the Baiyun Sag. Significant transgression from south to north influenced the depositional environment, resulting in large fluvial-dominated deltas and coastal deposits derived primarily from the northwestern provenance (Xiang et al., 2024). During this phase, the Yunkai Low Uplift was only partially exposed above water, resulting in reduced sediment supply. Sedimentation in the southwestern Baiyun Sag, primarily sourced from the Shunhe Uplift, was, characterized by shallow lacustrine and deltaic deposits.

3 Materials and methods

This study evaluates the reservoir potential of Enping Formation by integrating 3D seismic data with well logs and core data (including drilling and sidewall cores). The 3D seismic data enable paleogeomorphological reconstruction, third-order sequence division, amplitude attribute extraction, provenance determination, and seismic facies identification to define macroscopic sediment distribution. Well logs and core data support sedimentary microfacies characterization and analysis of key controls on reservoir property (Figure 2).

3.1 Seismic data

This study utilized 3D seismic data covering approximately 5,700 km^2, acquired with 12 × 6000 m streamer cables and a seismic source at 6 m depth (volume: 3,875 in^3). Data specifications: 5–40Hz bandwidth (dominant: 20 Hz), 15 × 12.5 m bin size, Enping Formation velocity: 2000–4,000 m/s, and theoretical vertical resolution: 25–50 m. Root mean square (RMS) attributes for sedimentary facies analysis were derived from pre-stack time migration (PSTM) data, while seismic interpretation and stratigraphic division were conducted using the pre-stack depth migration (PSDM) data.

3.2 Seismic sedimentology

1. Palaeogeomorphological Analysis: using interpreted horizons of the Enping Formation in the time domain, the residual thickness method was applied to reconstruct palaeotopography, thereby facilitating analysis of sediment transport pathways and the spatial distribution characteristics of sedimentary bodies.
2. Sequence Stratigraphic Analysis: Key geologic markers that are insensitive to seismic frequency variations, such as maximum flooding surfaces, unconformities, and initial flooding surfaces, are identified, correlated, and mapped to construct a seismic sequence framework for third-order sequences.
3. Seismic Phase Adjustment: a 90°-phase rotation was applied to the 3D seismic data to enhance well-to-seismic calibration, thereby clarifying the relationship between seismic reflections and lithology. This process provides a foundation for interpreting the planar distribution of sand bodies.
4. Seismic Attribute Analysis: on the basis of phase-adjusted data, sequence boundaries were used as reference horizons for the systematic extraction of seismic attribute slices. Integrated interpretation of sand body distribution and sedimentary facies was conducted to achieve detailed characterization of the delta–sub-lacustrine fan system.

3.3 Experimental methodology

1. Petrophysical properties (porosity/permeability) of 205 sidewall and drilling core samples were measured using a PoroPDP-200 overburden porosity-permeability system.

2. X-ray diffraction (XRD) analysis of 57 powdered samples (200-mesh) was conducted on a Bruker D8 Advance diffractometer (2°–70° scanning range), with mineral identification and quantification performed via Jade 6.5 software.
3. For pore-structure characterization, 48 sandstone samples were prepared as epoxy-impregnated thin sections through vacuum-pressure injection, followed by curing and polishing to 10.00 × 10.00 × 0.03 mm, These sections were then examined under a ZEISS AxioScope A1 APOL polarized microscope.
4. Mercury injection capillary pressure (MICP) tests included: ① High-pressure MICP (AutoPore IV 9600; 7 kPa–100 MPa; throat radius: 7.25 nm–105 μm; σ = 485 mN/m, θ = 130°) quantitatively characterizing pore-throat architecture on 1-cm^3 rock cubes dried >24 h at 80 °C; ② Constant-rate MICP (APSE-730; max 6.16 MPa/min throat radius 0.12 μm; 5 × 10^{-5} mL/min injection rate) enable pore-throat differentiation by detecting pressure fluctuations during quasi-static injection.
5. Pore-throat networks and clay morphology of 44 samples were characterized via scanning electron microscopy (LEO-435VP; 150–8×000 magnification) under controlled conditions (20 °C, 50% RH).

All experimental analyses were conducted by the CNOOC Experimental Center under CNOOC Energy Technology & Engineering Services Co., Ltd.

4 Results

4.1 Paleogeomorphological Characteristics

Paleogeomorphology provides the primary control on source-to-sink systems, governing sediment transport pathways and depositional sinks. It determines the distribution of sediment sources and spatial sediment distribution patterns during periods (Xu et al., 2004; Deng et al., 2001). Common paleogeomorphological reconstruction methods include residual thickness method, filling-mold techniques, and sequence stratigraphic analysis (Pang et al., 2013). Based on seismic and drilling data, the paleogeomorphology during the Enping Formation deposition was reconstructed in the study area using the residual thickness method.

Paleogeomorphological mapping and seismic profiles from the Enping Formation depositional period reveal three prominent uplift zones: Shunhe Uplift, Yunkai Low Uplift, and Baiyun South Low Uplift. The depressional troughs between these uplifts served as primary conduits for long-distance sediment transport. The trough morphology between the Yunkai Low Uplift and Baiyun South Low Uplift indicates west-to-east sediment transport during deposition of the fourth member of the Enping Formation, with the L13 area as the depocenter. Simultaneously, the low-relief zone between the Shunhe Uplift and Yunkai Low Uplift functioned as a local sediment convergence area (Figure 3).

4.2 Sedimentary facies distribution and Sequence Architecture

4.2.1 Sedimentary facies types

Integrated analysis reveals braided river delta dominance in the Enping Formation, characterized by four microfacies.

4.2.1.1 Subaqueous distributary channel microfacies (braided delta front)

Lithology: Grayish-green fine-medium sandstones exhibit well-developed lenticular bedding and high-angle cross-bedding,along with glauconite enrichment, intense bioturbation (Figure 4), and vigorous acid reaction.

Log Response: Low-amplitude gamma-ray (GR) log patterns showing funnel-to-bell shapes, with gradational top and basal contacts.

Seismic Characteristics: Displays medium-amplitude, "U"-shaped incised channels with stacked geometries (Figure 5).

4.2.1.2 Distal bar microfacies (braided delta front)

Lithology: Dominated by grayish-green medium-to fine-grained sandstones.

Basal Unit: Massive sandstones with horizontal bedding and localized calcareous enrichment, vigorous effervescence occurs with acid treatment.

Middle Unit: Thick (~2 m) fine-grained sandstones with lenticular bedding.

Upper Unit: Calcite-rich, horizontally bedded fine-grained sandstones exhibiting load casts and soft-sediment deformation (Figure 4).

Log Response: Inverse grading (funnel-shaped GR log), abrupt upper contact, and gradational basal boundary.

Seismic Characteristics: Parallel, moderately continuous, medium-amplitude reflections (Figure 5).

4.2.1.3 Braided channel microfacies (braided delta plain)

Lithology: Light gray pebbly coarse-grained sandstones with quartz granules (2–4 mm diameter). Minor pyrite and calcareous fragments are present, vigorous effervescence occurs with acid treatment.

Log Response: Low-amplitude, slightly serrated bell- or box-shaped GR curves, reflecting frequent channel avulsion. Sharp upper and basal contacts.

Seismic Characteristics: High-amplitude, parallel sheet-like reflections (Figure 5).

4.2.1.4 Sublacustrine fan channel microfacies

Lithology: Light gray fine-grained sandstones in massive beds (up to 35 m thick). Calcareous cementation increases downward, with vigorous acid reaction.

Log Response: Slightly serrated box-shaped GR log with sharp top and basal boundaries.

Seismic Characteristics: Toothed parallel reflections with medium-to-low amplitudes (Figure 5).

4.2.2 Sequence Architecture

In the 1970s, Exxon's research utilizing 2D seismic data demonstrated that seismic reflection termination patterns could

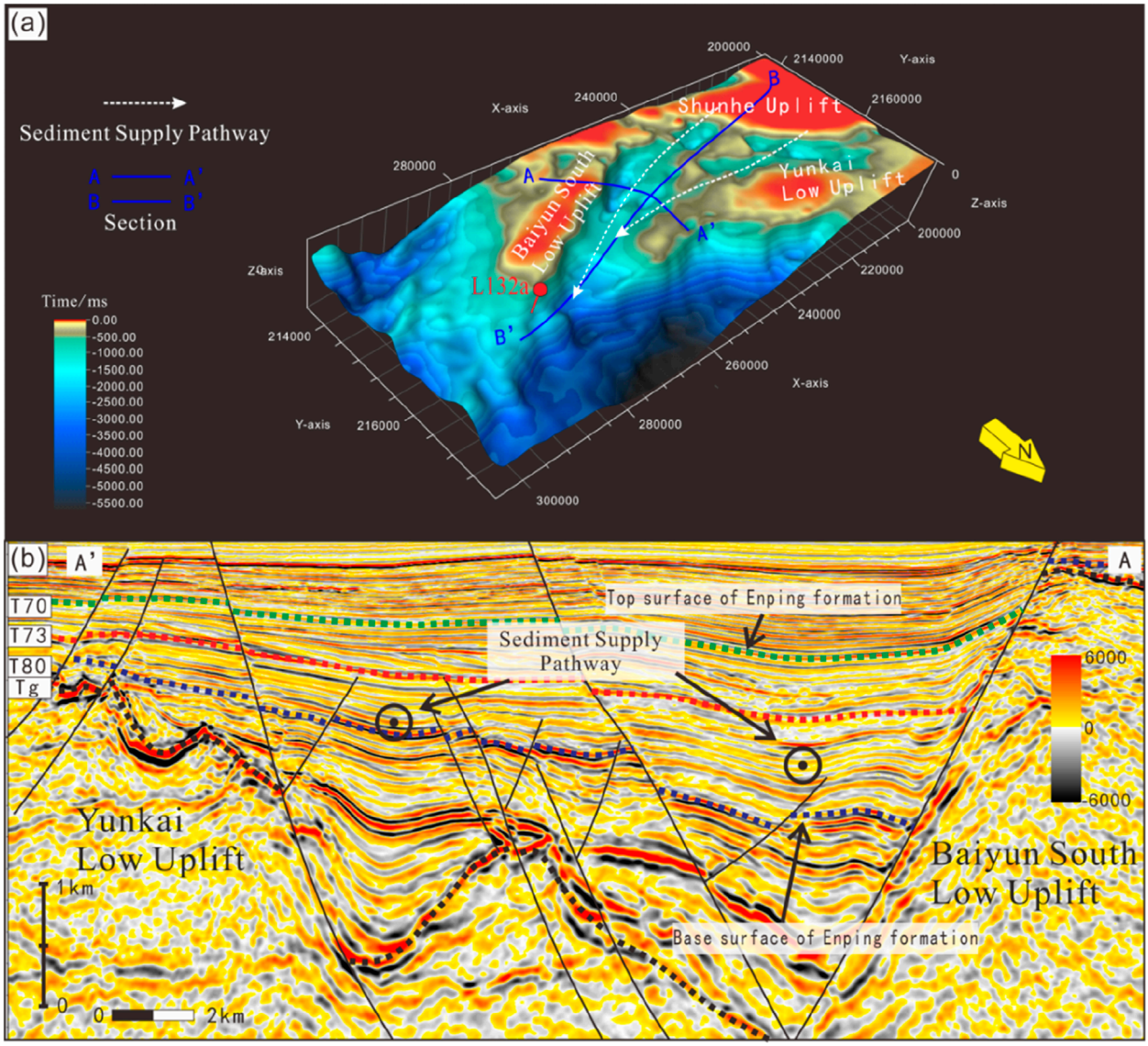

FIGURE 3
(a) Isochron map and **(b)** paleogeomorphological characteristics of the Enping formation (Figure 1b A-A′).

predict the distribution of source rocks, reservoirs, and seals (Mitchum et al., 1977; Vail et al., 1977). This breakthrough established seismic stratigraphy, giving rise to the conceptual framework of depositional sequences—genetically linked stratigraphic units bounded by unconformities and their correlative conformities. Two sequence models were defined: Type I Sequences develop when base-level fall drops below the shelf-edge, containing lowstand systems tract (LST), transgressive systems tract (TST), and highstand systems tract (HST); Type II Sequences form when base-level remains above the shelf-edge. This Type I tripartite architecture represents the third-order sequence model applied in this study, whereas Type II is not utilized.

In the study area, two third-order sequences are identified within the Enping Formation: EPSQ2 (third member) and EPSQ1 (fourth member) (Figure 6). Sequence boundaries (SB) exhibit truncation and toplap features at upper interfaces. Basal boundaries display downlap features in slope-to-basin settings. And three key SB are identified: T80, T73, and T70. Maximum flooding surfaces (MFS1 and MFS2) are identified beneath strata displaying apparent truncation at their upper contacts. The initial flooding surface (IFS) is delineated by the first onlap termination. Based on these surfaces, the sequences EPSQ1 and EPSQ2 are subdivided into TST, HST, and LST.

In the lacustrine shelf zone, seismic reflections are characterized by parallel to sub-parallel and progradational configurations. Parallel to sub-parallel reflections typically indicate stable hydrodynamic conditions, with upward-shortening seismic events reflecting retrogradational stacking and lake-level rise. Progradational reflections suggest sediment delivery toward the basin center, often corresponding to lake-level fall. In the slope-to-basinal zone, seismic facies include sigmoid progradational and dish-shaped reflections, and dish-shaped reflections with bidirectional downlap signatures are considered as sublacustrine fan deposits.

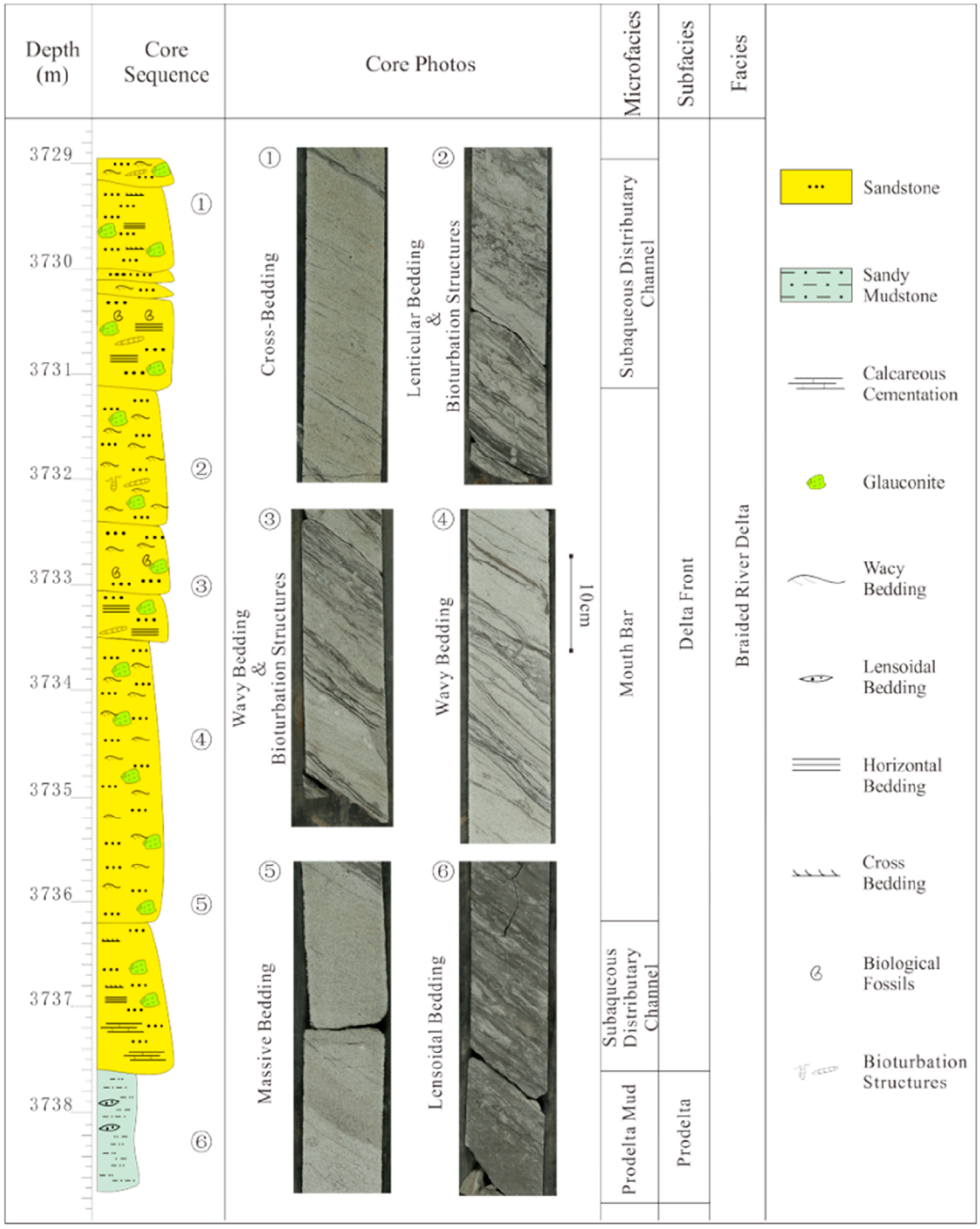

FIGURE 4
Drilling core sequence from 3,728.95 to 3,738.78 m in Well L132a.

4.3 Seismic depositional facies analysis

4.3.1 90° phase rotation

The 90° phase rotation is one of the key techniques in seismic sedimentology studies. Conventional seismic processing produces zero-phase data, whose seismic events reflect the acoustic impedance contrasts at formation interfaces but provide no direct indication of lithology. In contrast, seismic sedimentology relies on establishing a relationship between seismic events and lithology. By applying a 90° phase rotation, the central lobe of the seismic response is shifted to correspond with sand bodies, thereby creating a link between seismic events and sand deposition (Zhu et al., 2011). This process ultimately assigns geological meaning to the seismic events.

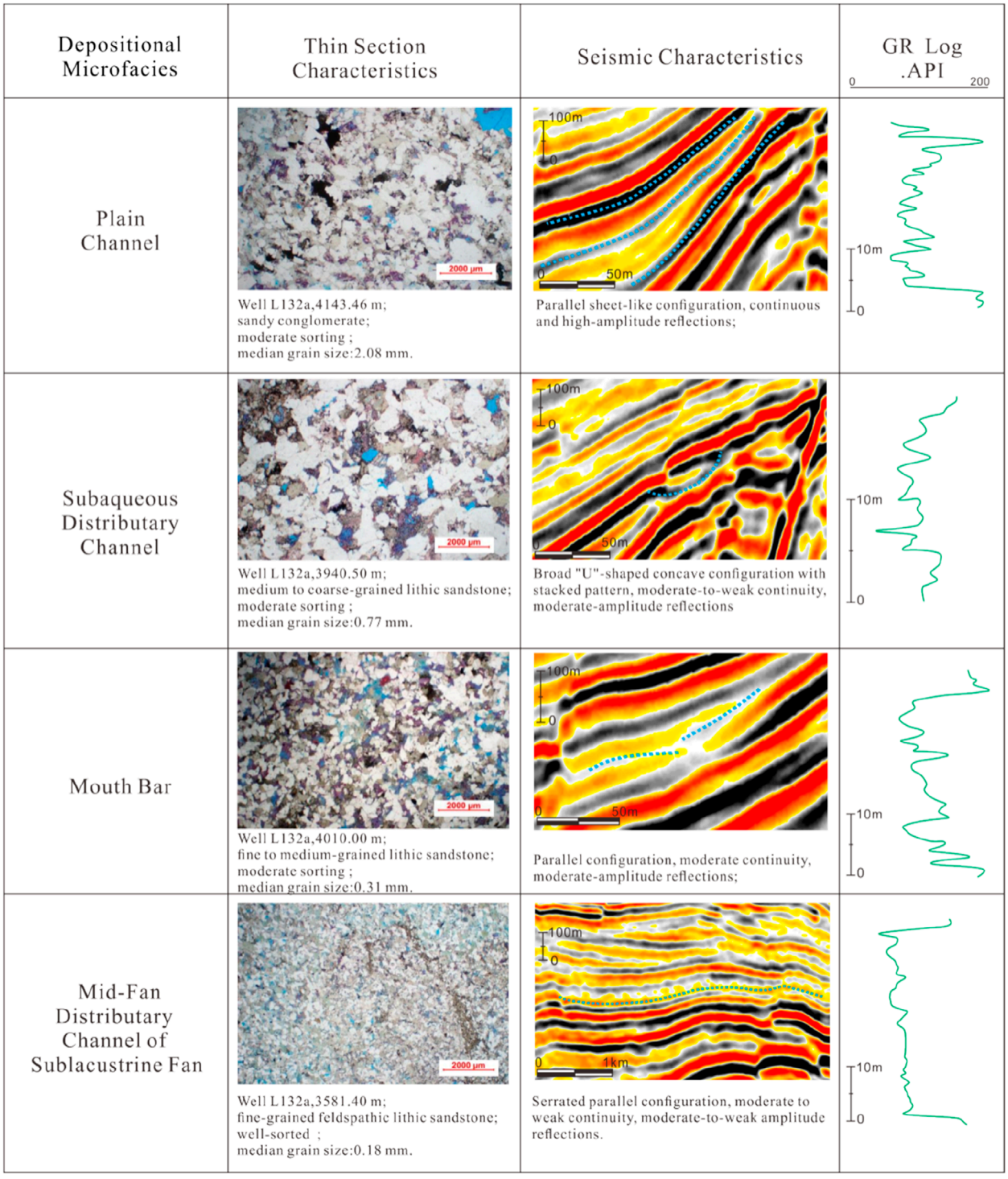

FIGURE 5
Characteristics of depositional microfacies types in the Enping formation.

The applicability of the 90° phase rotation technique in this study area requires experimental validation to confirm its reliability. Synthetic seismograms can establish a correlation between well logs and seismic data. Based on this correlation, the density (DEN) log—effectively reflecting lithological variations in the area—was used for well-to-seismic calibration tests. As demonstrated by the calibration from well L132a (Figure 7a), the zero-phase seismic section shows no consistent correspondence between sandstone intervals (identified by the density log) and seismic phases. In contrast, the 90° phase-rotated section shows a strong correlation between well logs and seismic events: sandstones predominantly correspond

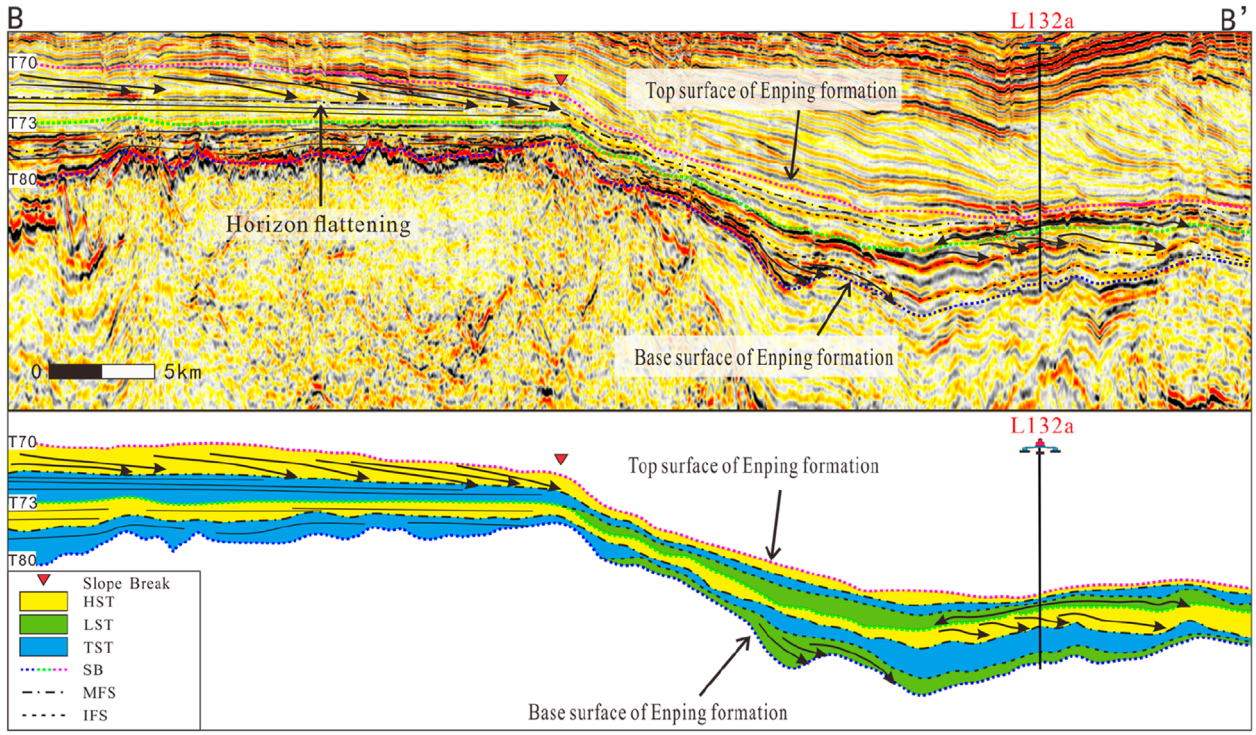

FIGURE 6
Sequence architecture of the Enping formation (Figure 1b B-B′).

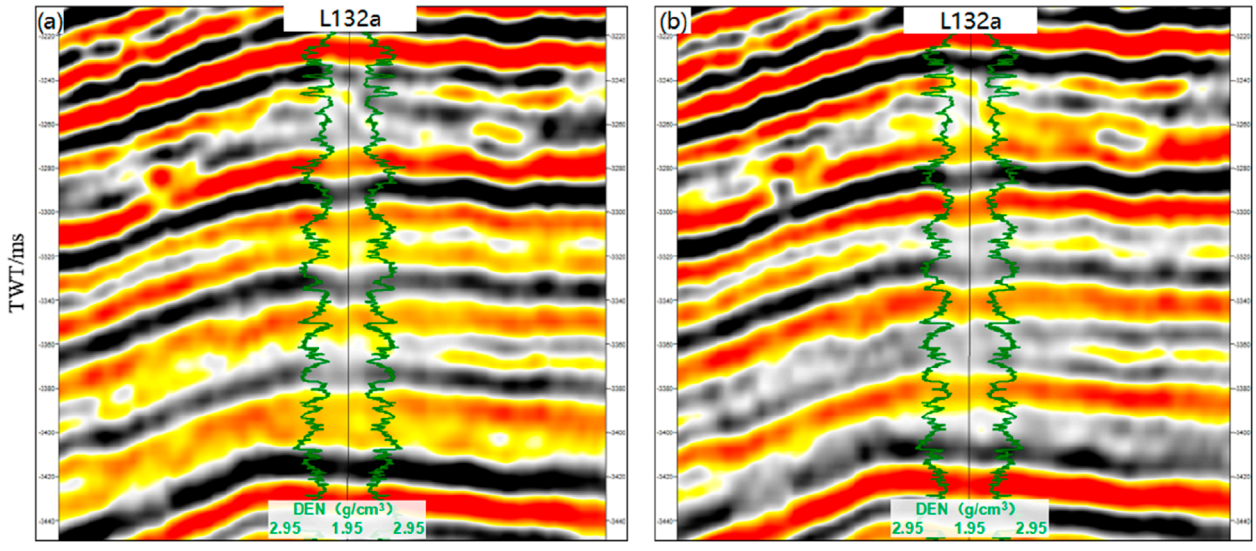

FIGURE 7
The relationship of well-seismic data between zero phase profile **(a)** and 90° phase shift profile **(b)** through well L132a.

to red peaks, while mudstones are largely associated with black troughs (Figure 7b).

4.3.2 Interpretation of stratal slice

Regarding the geometric characteristics of clastic sedimentary bodies, individual sedimentary sand bodies are characterized by a lateral extent far exceeding their vertical dimension (Galloway and Hobday, 1983). Meanwhile, studies have shown that the vertical and horizontal resolutions of 3D seismic data are roughly equivalentt (Lindsey, 1989). The stratal slice technique—applied within a sequence stratigraphic framework—utilizes lateral variations in seismic attributes to identify facies changes, thereby

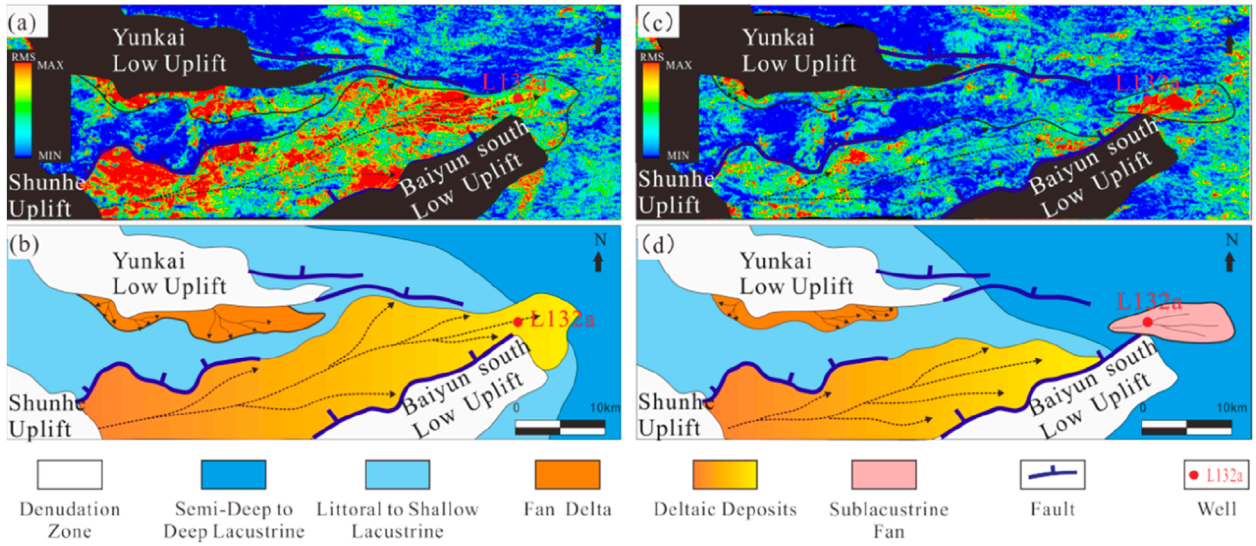

FIGURE 8
RMS Amplitude Attributes and Sedimentary Facies Maps of the Third and Fourth Members of the Enping Formation in Block L13. **(a)** RMS amplitude attribute of the Fourth Member (60 ms window below from T73); **(b)** Sedimentary facies map of the Fourth Member; **(c)** RMS amplitude attribute of the Third Member (40 ms window upward from T73); **(d)** Sedimentary facies map of the Third Member.

compensating for the limitations of vertical resolution in planar view. Based on the established sequence stratigraphic framework, the generation and application of stratal slices enable the analysis of the evolution of sedimentary systems and the distribution of facies belts.

Based on the 90° phase-rotated seismic data, RMS amplitude stratal slices effectively reveal the distribution and boundaries of depositional facies within the study area. Using T73 as a reference surface, this study extracted and analyzed RMS amplitude attributes for HST and LST. Higher RMS values indicate higher sand content, whereas lower values correspond to higher mud content. This analysis enabled the differentiation of sand and mud distribution patterns for the HST and LST (Figures 8a,c), thereby clarifying the evolutionary process from braided river delta deposits during the HST (Figure 8b) to sublacustrine fan deposits during the LST (Figure 8d).

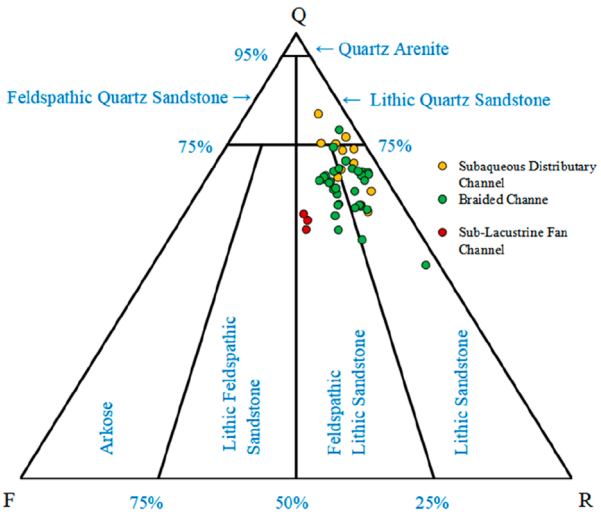

FIGURE 9
Compositional classification of sandstones in the Enping formation.

4.4 Reservoir characteristics

4.4.1 Petrological characteristics

Thin-section analysis indicates that the Enping Formation reservoirs are primarily feldspathic litharenite and litharenite (Figure 9).

The braided channel microfacies is primarily composed of litharenite, exhibiting moderate compositional maturity (Q/(F + R) = 1.5–4.6, avg. 2.6) with detrital components of quartz (60.0–82.0%, avg. 70.8%), lithics (13.0–33.0%, avg. 23.5%), and feldspar (2.5–8.6%, avg. 5.7%). Coarse-grained to pebbly sandstones, subangular-subrounded grains, and long-concave-convex contacts indicate poor textural maturity under intense compaction.

The subaqueous distributary channel microfacies comprises both lithic arkose and litharenite, showing moderate compositional maturity (Q/(F + R) = 0.9–3.6, avg. 1.9) with quartz (48.0–78.4%, avg. 65.3%), lithics (18.6–49.5%, avg. 26.6%), and feldspar (2.5–14.4%, avg. 8.1%). Medium-coarse sandstones with point-long contacts suggest proximal deposition.

The sublacustrine fan channel microfacies is characterized by feldspathic litharenite with low compositional maturity (Q/(F + R) = 1.3–1.5, avg. 1.4), evidenced by high feldspar (18.8–20.2%, avg. 19.3%) and low quartz content (56.0–59.5%, avg. 57.9%). Fine-grained sandstones, subrounded grains, and dominant long contacts suggest distal transport and high textural maturity.

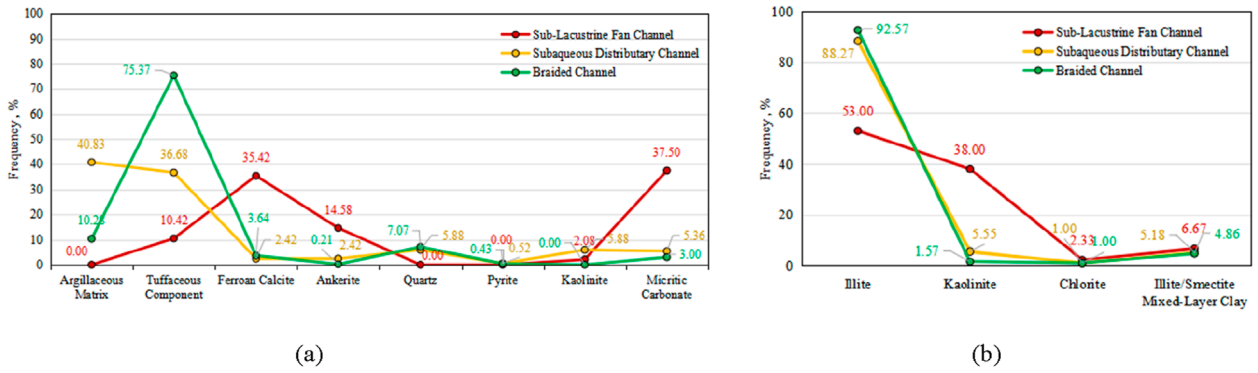

FIGURE 10
Characteristics of Reservoir Matrix Composition in the Enping Formation. **(a)** Histogram of interstitial material composition. **(b)** Histogram of clay mineral composition.

Mineral composition and XRD reveals pronounced facies-controlled interstitial material distribution (Figure 10a). The braided channel microfacies contains exceptionally high tuffaceous material (75.37%), whereas the subaqueous distributary channel microfacies shows moderate levels (36.68%). These tuffaceous components provide essential material for fluid-driven alteration. Their concentration differences directly control secondary dissolution intensity—ultimately impacting reservoir properties. Both facies exhibit significant illite among clay minerals (Figure 10b), which clogs pore throats during diagenesis and and reduces permeability. In contrast, the sublacustrine fan microfacies has minimal tuffaceous content (10.42%) but develops substantial carbonate cement (37.50%), indicating pore-occluding cementation that severely degrades pore networks.

4.4.2 Petrophysical characteristics

Analysis of 70 drilling core and sidewall core samples from the Enping Formation reveals that the reservoirs generally exhibit moderate to low porosity (6.6–21.1%, median: 14.6%) and low-ultralow permeability (0.02–21.30 mD, median: 0.60 mD).

Sandstones in the braided channel microfacies exhibit porosity of 12.3%–18.6%, with modal concentration in the 10–15% range (63.64% frequency) and 36.36% exceeding 15% (Figure 11a). Permeability ranges from 0.03 to 5.41 mD, predominantly within 0.1–10 mD (Figure 11b). 36.36% of values exceed 1.0 mD, indicating low-permeability reservoir characteristics.

The subaqueous distributary channel microfacies displays broader porosity (6.6–22%, median 14.6%), with 47.37% exceeding 15% (Figure 11a). Permeability ranges from 0.02 to 21.3 mD, showing modal concentration in 0.1–10 mD (Figure 11b), and 43.86% exceed 1.0 mD, classifying these as moderate-to-low permeability reservoirs.

In contrast, sublacustrine fan channel sandstones exhibit 11.2–14.5% porosity but permeability consistently <0.1 mD (Figure 11b), characteristic of tight-reservoir behavior.

A porosity-permeability cross-plot on logarithmic coordinates shows a strong positive correlation (R^2 > 0.5), with permeability showing an exponential growth trend as porosity increases (Figure 12), confirming porosity-dominated reservoir behavior. Certain data points deciate significant from this trend, demonstrating enhanced permeability at similar porosity levels, which indicates positive reservoir modification by secondary dissolution processes.

Despite generally poor petrophysical properties, approximately 40% of reservoirs exhibit moderate porosity (>15%) and permeability (>1mD). Given the Baiyun Sag's high geothermal gradient and the industry's growing focus on low-permeability gas plays (Ma et al., 2024), the Enping Formation holds significant exploration potential for low-permeability gas accumulations.

4.4.3 Pore types and throat characteristics

Thin-section and SEM analyses reveal the Enping Formation reservoirs are dominated by intergranular and intragranular dissolution pores, with primary porosity significantly reduced by intense compaction. Strong dissolution has reshaped pore systems: widespread dissolution of tuffaceous material, feldspars, and rock fragments creates interconnected intergranular pores (Figure 13a), while selective leaching of mineral grains forms intragranular and moldic pores (Figure 13b). Additionally, authigenic clay minerals (e.g., illite, kaolinite) derived from tuff or feldspar dissolution create intercrystalline micropores (Figure 13c). SEM observations further reveal secondary dissolution pores on quartz surfaces, alongside honeycomb-like illite/smectite (I/S) mixed-layer clays and Type III illite with abundant stacked kaolinite aggregates (Figure 13d). Pervasive pore-filling cements—fibrous illite, booklet-like kaolinite, I/S clays, and blocky carbonates (Figures 13e,f), granular ferroan calcite, micritic siderite, and framboidal pyrite—reduce effective porosity and degrade pore connectivity, particularly throat radii. The reservoirs exhibit a dual-porosity network: dissolution-enhanced macropores and clay-associated micropores. Low pore-throat ratios result in high capillary trapping, defining the Enping Formation as a typical secondary reservoir.

MICP curves indicate that the Enping Formation sandstones exhibit low displacement pressures (0.138–0.67 MPa, avg. 0.33 MPa) and mercury injection permeability ranging from 0.11 to 15.8 mD (avg. 2.64 mD) (Figure 14a). Throat radius distributions show a median throat radius (R50) of 0.084–0.56 μm (avg. 0.26 μm) (Figure 14b), classifying the throats as submicron-scale

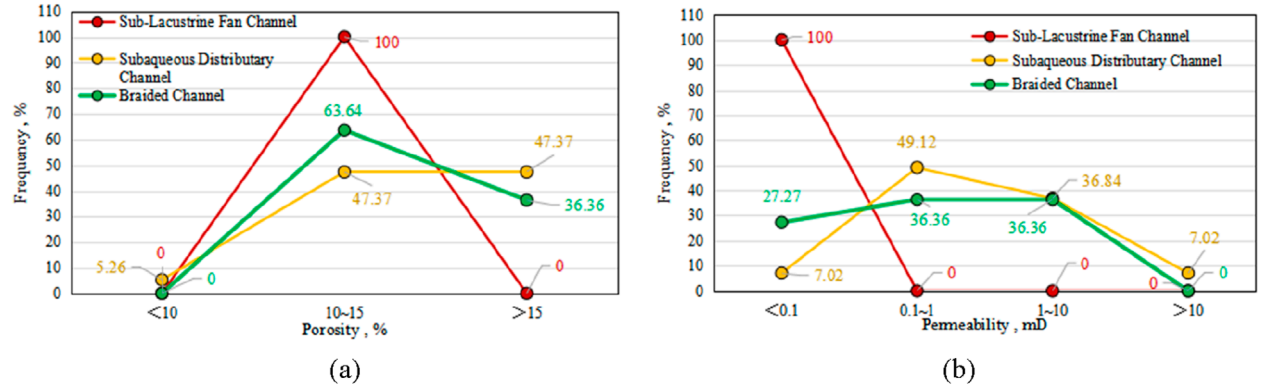

FIGURE 11
Petrophysical Properties of the Enping Formation Reservoirs. **(a)** Porosity distribution histogram. **(b)** Permeability distribution histogram.

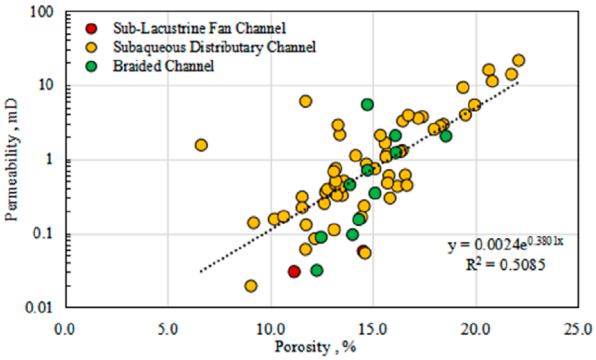

FIGURE 12
Porosity-permeability correlation of the Enping formation reservoirs.

with a sorting coefficient (Sp) of 2.9–3.8. The steeply inclined MICP curves and short plateau segments reflect poor throat sorting and low mercury withdrawal efficiency (19.4–31.6%, avg. 24.9%), collectively indicating inferior reservoir quality.

Although intergranular and intragranular dissolution pores are well-developed, reservoir performance is severely compromised by inefficient throat networks dominated by neck-shaped, lamellar, and tubular throats (Figures 13g–i). These complex throat geometries restrict pore connectivity, while pervasive infilling of illite and kaolinite within pores and throats further diminishes both storage capacity and fluid mobility. The interplay of dissolution-enhanced porosity and throat occlusion by diagenetic minerals defines a high-storage, low-deliverability reservoir system, characteristic of tight sandstone reservoirs.

5 Discussion

Depositional processes exert dual controls on reservoir development: macroscopically governing the spatial distribution and scale of sedimentary bodies, and microscopically dictating sediment grain size, composition, and primary pore architecture. These factors collectively determine reservoir heterogeneity, leading to significant performance variations across different depositional settings. Concurrently, diagenesis modifies sediment composition and texture under varying physico-chemical conditions, ultimately controlling the porosity and permeability of reservoir units (Wang et al., 2019; Yang et al., 2007; Zhou et al., 2008).

5.1 Sedimentary evolution and modern depositional analog

Integrated analysis incorporating paleogeomorphology, sequence stratigraphy, and RMS amplitude attribute slices clarifies the distribution characteristics of deltas and sublacustrine fans in the third and fourth members of the Enping Formation (Figure 8).

5.1.1 Deposition of the fourth member (EPSQ1, HST)

During this highstand systems tract, the Shunhe Uplift served as the dominant provenance, supplying abundant sediment. Sediments were transported through nearly E-W trending fault-bounded troughs to topographic lows, forming large-scale deltaic systems, These deltas exhibit strong paleotopographic control, characterized by elongated geometries parallel to trough axes and lateral confinement by bounding faults.

5.1.2 Deposition of the third member (EPSQ2, LST)

Under lowstand conditions, deltas retreated landward. Influenced by a west-to-east topographic gradient, sublacustrine fans developed in distal basin settings.

The study area developed a braided delta system. Systematic analogy with modern coarse-grained braided deltas (Figure 15a) reveals seismic RMS responses to facies differentiation: (1) Delta-plain high-energy braided channels (shallow geometries, frequent migration) form clustered amalgamated bar complexes (Figure 15b①-②), corresponding to high RMS amplitudes marking sandy aggradational centers from channel avulsion; (2) Delta front isolated lobes along subaqueous distributary channel exhibit mottled low RMS responses (Figure 15b③), indicating

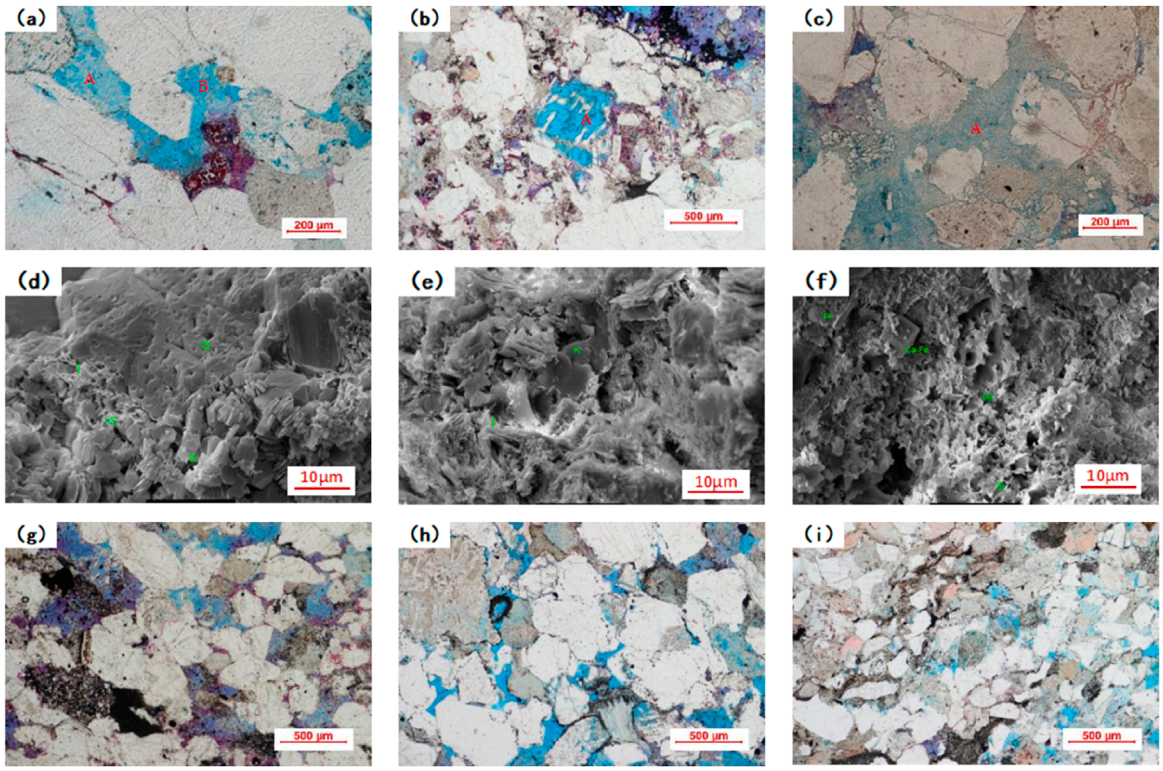

FIGURE 13
Pore System Characteristics of the Enping Formation Reservoirs. **(a)** 3,762.00 m, intercrystalline pores **(a)** and intergranular dissolution pores **(b)**; **(b)** 4,246.27 m, fully dissolved moldic pores **(a)**; **(c)** 4,053.00 m, authigenic clay minerals and intergranular dissolution pores **(a)**; **(d)** 3,581.4 m: secondary dissolution pores; **(e)** 3,940.5 m: Stacked kaolinite and Type III illite; **(f)** 3,967.4 m: Honeycomb illite/smectite mixed-layer clays; **(g)** 3,997.10 m: Tuffaceous dissolution and neck-shaped throats; **(h)** 3,729.39 m: Dissolution pores and lamellar throats; **(i)** 3,729.13 m: intragranular dissolution pores with tubular throats.

mud-partitioned sand dispersal. This coarse-grained sediment-load system responds to basin-margin topography, with facies partitioning jointly governed by topographic confinement and flow energy. The modern analog provides critical sediment-dynamic constraints for seismic attribute interpretation.

5.2 Impact of depositional processes on reservoir quality

RMS amplitude slices reveal the sedimentary response from the HST to the LST of a braided delta–sub-lacustrine fan system (Figures 8A,C). High RMS amplitudes correspond to more extensive sand deposition, while channel avulsion and variations in sediment supply resulted in the accumulation of sand bodies with different thicknesses in different areas.

During the HST period, the widespread distribution of high RMS amplitudes indicates active deltaic systems with strong sediment supply from the Shunhe Uplift. The sediments prograded over considerable distances, forming large-scale braided delta deposits. The east-to-west lateral decrease in RMS amplitude reflects a gradual reduction in clastic sediment accumulation with increasing transport distance, as well as the transition from delta plain to delta front facies (Figure 8b).

In the LST phase, the overall RMS amplitude is significantly weaker compared to the HST (Figure 8c). High amplitudes are more scattered and limited in extent, suggesting shorter transport distances during lake-level rise and westward contraction of the delta system. Influenced by topographic slope (Figure 3a), fine-grained sub-lacustrine fan deposits developed in the lake basin. The relatively high RMS amplitude of these fans not only reflects depositional scale but also indicates the distinct composition of the sand bodies (see Chapter 5.3).

The spatial variation in RMS amplitude, indicative of transport distance and facies zonation, exerts a primary control on the scale, grain size, and sorting of sand bodies, thereby further influencing reservoir quality.

Statistical analysis of sedimentary microfacies, lithology, grain size, petrophysical properties, and pore types in the Enping Formation reveals systematic reservoir quality variations controlled by depositional environments. The braided delta plain channel microfacies, characterized by conglomerates and poorly to moderately sorted coarse-grained sandstones, exhibits moderate dissolution porosity (intergranular pore area: 0.5–6.5%, avg. 2.9%) but low reservoir quality (avg. porosity: 14.8%, permeability: 1.14 mD), which is attributed to high tuffaceous content (avg. 13.2%). In contrast, the braided delta front subaqueous distributary channel microfacies, dominated by moderately sorted medium-to-coarse sandstones, demonstrates superior reservoir potential due

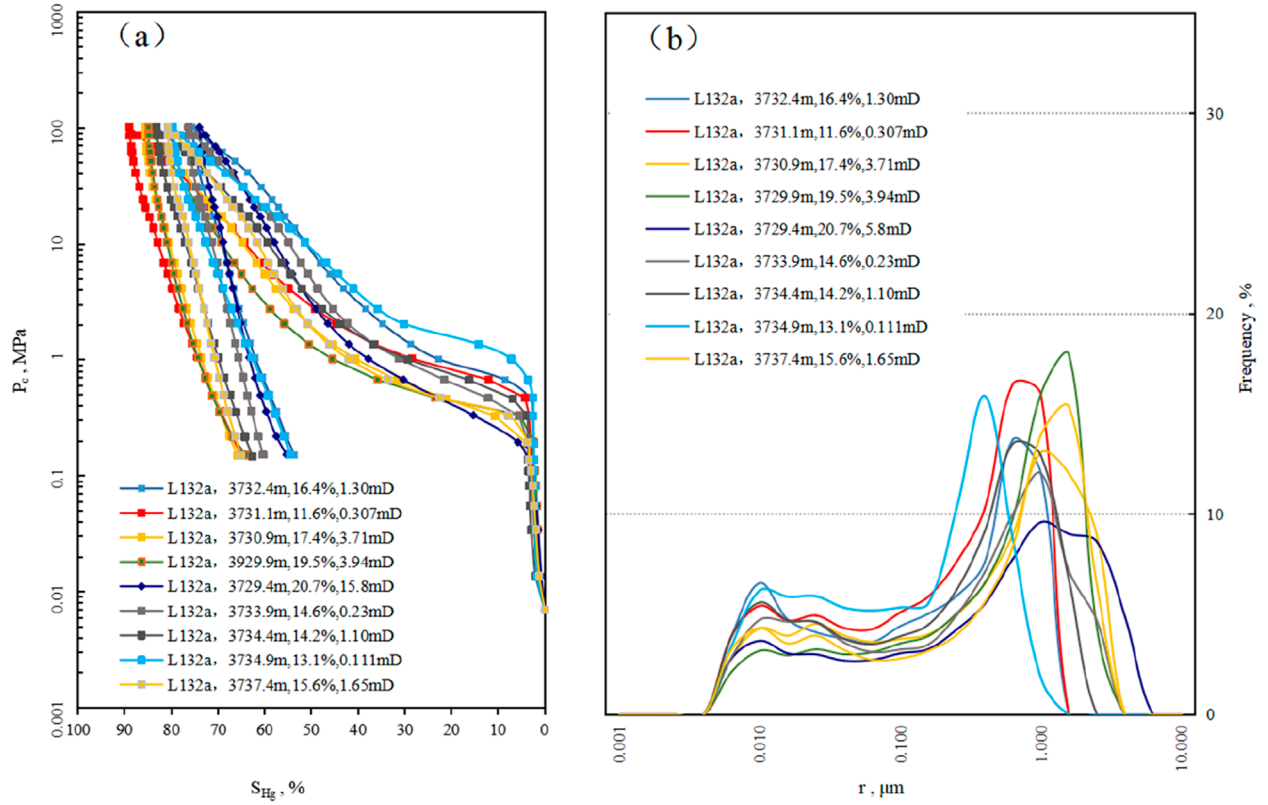

FIGURE 14
Pore Structure Characteristics of the Enping Formation Reservoirs. **(a)** Mercury Injection Capillary Pressure (MICP) curve of the Enping Formation in Well L132a. **(b)** Pore-throat radius distribution curve of the Enping Formation in Well L132a.

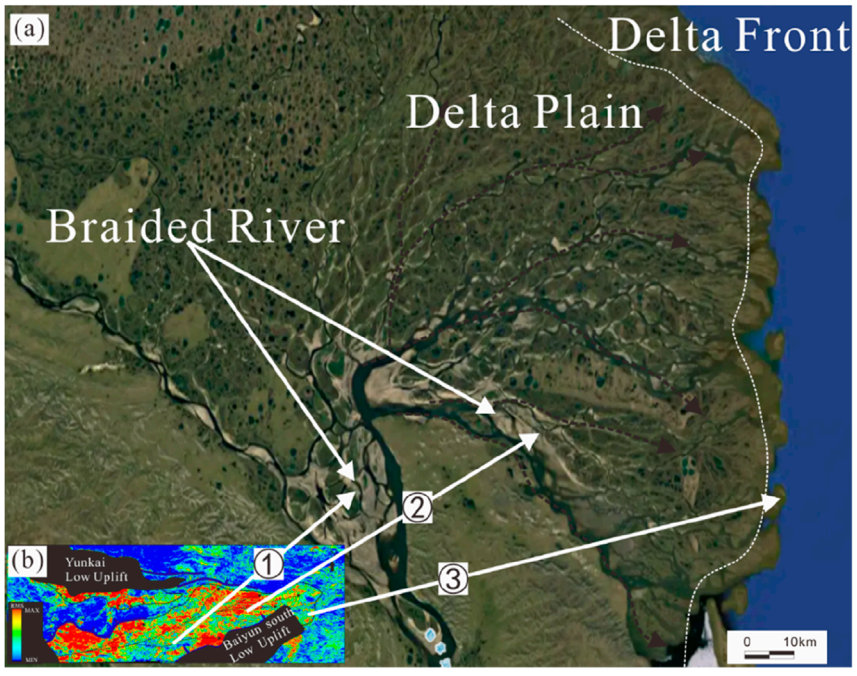

FIGURE 15
Modern Braided Delta Analog. **(a)** Lena River Braided Delta (E128.6°,N72.6°); **(b)** RMS amplitude attribute of the Fourth Member.

to abundant intergranular dissolution pores (pore area: 1–17%, avg. 7.1%), lower tuffaceous content (avg. 8.4%), and enhanced petrophysical properties (avg. porosity: 16.6%, permeability: 4.95 mD), establishing it as the primary facies. Conversely, the mid-fan sublacustrine fan channel microfacies, comprising of well-sorted fine-grained sandstones, shows limited dissolution porosity (pore area: 1–5%, avg. 2.7%) and ultra-low permeability (avg. 0.04 mD) despite moderate porosity (avg. 12.9%). This facies-dependent hierarchy—where delta front channels exhibit optimal porosity-permeability (partially reaching moderate levels), delta plain channels display low-quality characteristics, and sublacustrine fan channels represent the poorest reservoirs—definitively establishes that depositional facies govern both lateral and vertical reservoir heterogeneity in the Enping Formation of the L13 area, with hydrodynamic energy, sediment sorting, and tuffaceous content acting as key controlling factors.

5.3 Impact of diagenesis on reservoir quality

Research demonstrates that compaction and cementation constitute the predominant destructive diagenetic processes in the L12 area, whereas dissolution acts as the principal constructive diagenetic mechanism in the L13 area. Compaction, identified as the primary factor degrading reservoir quality, exhibits a dominant depth-dependent control: in shallow reservoirs (<2,500 m burial depth), favorable petrophysical properties prevail, characterized by moderate to high porosity (up to 28.2%) and permeability (up to 599 mD), with thin-section observations revealing point-floating grain contacts and a maximum visible pore area of 26% (Figures 16a,b). In contrast, deeper reservoirs (>2,500 m) experience significant quality deterioration, with porosity mostly below 15%, permeability less than 1 mD, and grain contacts transitioning to concave-convex and line types under compaction (Figure 16c). Calculations based on unconsolidated sandstone porosity models (Beard and Weyl, 1973; Wang et al., 2024) reconstruct an average initial porosity of 51.8% for the L132a unit, with mechanical and chemical compaction accounting for 87.4% porosity loss. This depth-controlled compaction gradient, evidenced by progressive grain rearrangement and pore collapse, unequivocally establishes intense compaction as the dominant mechanism driving reservoir degradation in deeply buried intervals, while shallow reservoirs retain relatively preserved pore networks due to limited diagenetic overprinting.

Cementation, commonly recognized as a critical factor degrading reservoir quality (Jiang et al., 2004; Li et al., 2005), exhibits limited intensity in the Enping Formation of the L13 area, with an average visible cementation rate of merely 4.5% based on thin-section analysis. The cements predominantly comprise carbonate minerals (e.g., ferroan calcite, micritic carbonate) and authigenic clay minerals.

Submarine fan systems typically exhibit high RMS amplitude responses, with amplitude variations primarily reflecting changes in acoustic impedance. Based on well log data, relationships among different lithological properties—including acoustic impedance, clay content, and effective porosity—were analyzed (Figure 17). Under comparable clay content conditions (Figure 17a), calcareous sandstones show significantly higher acoustic impedance values than conventional sandstones (Figure 17b). Meanwhile, the influence of carbonate cementation results in inferior petrophysical properties in calcareous sandstones (Figure 17c). The high density and acoustic impedance characteristics of these rocks ultimately contribute to their strong RMS amplitude response.

In contrast, as identified in petrographic analysis (Chapter 4.4), sublacustrine fan channel sandstones contradict this trend, displaying elevated cement contents of 13–20%, dominated by dense carbonate cements (ferroan calcite and micritic carbonate). This anomalously high cementation—occurring despite favorable sorting and low clay content in these fan facies—directly contributes to their poor reservoir performance, as carbonate cements occlude intergranular pores and block fluid pathways. The high textural maturity fails to enhance permeability due to pervasive pore-filling diagenesis.

Dissolution represents the principal control governing the moderate-to-low porosity-permeability reservoir development in the tight Enping Formation of the L13 area. Its genesis is predominantly associated with organic acids expelled from deep source rocks: as burial depth increases and formation temperature remain elevated, organic matter within source rocks progressively matures. During thermal degradation, this organic matter undergoes extensive decarboxylation, generating organic acids and carbon dioxide. The organic matter in source rocks of the Wenchang and Enping Formations has already reached the mature to high-mature stage (Gao et al., 2024b; Zhang et al., 2025). During thermal evolution, significant volumes of organic acid fluids enriched with carbon dioxide are expelled. These fluids migrate along multiple faults connecting to the source rocks into the Enping Formation reservoirs within the target area. Subsequently, by dissolving soluble components—including tuffaceous matrix, feldspar, and lithic fragments—the fluids effectively enhance reservoir space (Figures 13a–c). These dissolution pores, manifested as feldspar dissolution pores, lithic dissolution pores, and tuffaceous dissolution pores, are widely observed in both delta plain channels and delta front distributary channel reservoirs. Thin-section analyses reveal that dissolution pores constitute 20–100% of total visible porosity (average 89.9%), confirming their dominance as the primary pore contributors in the Enping Formation. Critically, permeability enhancement depends fundamentally on both dissolution targets and resultant pore geometry evolution. For instance, intergranular tuffaceous dissolution pores (Figure 13h) develop well-connected pore networks after dissolution, achieving permeability values as high as 15.8 mD, whereas intragranular dissolution pores (Figure 13b) remain isolated, resulting in permeability as low as 0.088 mD. This marked disparity underscores that pore connectivity, governed by the spatial architecture of dissolution features, persists as the decisive controlling factor for permeability enhancement even in dissolution-dominated karst systems.

5.4 Developmental Model of reservoirs

Integrated analysis of sedimentary microfacies, reservoir characteristics, and diagenesis reveals key controls on reservoir development in the regionally tight Enping Formation. The

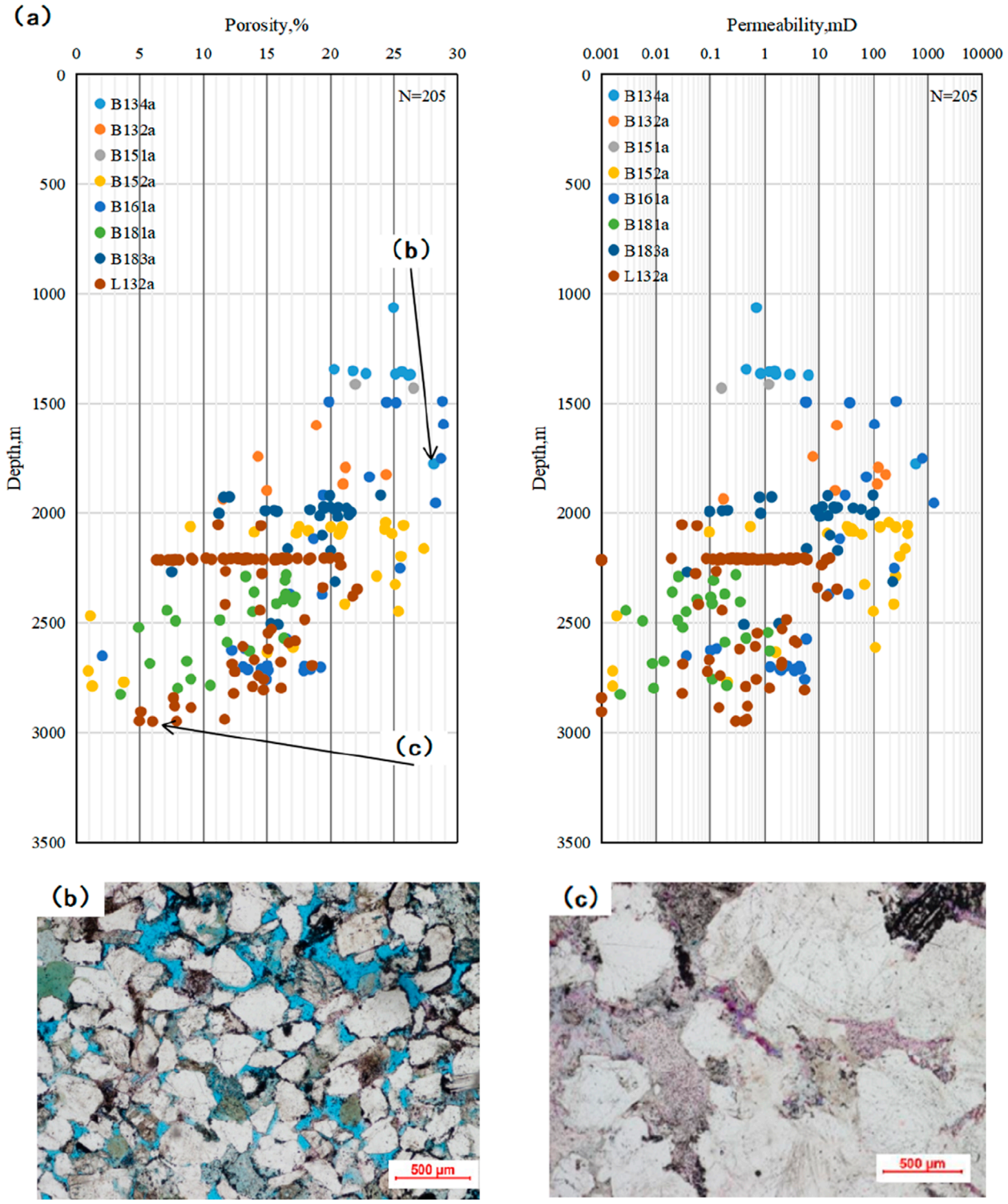

FIGURE 16
Compaction Evolution of Reservoirs in the Southwestern Baiyun Sag. **(a)** Correlation between burial depth and petrophysical properties; **(b)** Well B134a, burial depth 1776 m, porosity 28.2%, permeability 599 mD, point-floating grain contacts; **(c)** Well L132a, burial depth 2,949 m, porosity 7.9%, permeability 0.413 mD, concave-convex to line grain contacts.

subaqueous distributary channel microfacies of the braided delta front develops in the HST (Figure 18), exhibiting coarse-grained textures and intense dissolution modification. Its reservoir quality is governed by depositional-diagenetic coupling: Coarse-grained frameworks effectively preserve primary porosity systems, while fault-derived acidic fluids drive selective dissolution of tuffaceous matrix and unstable mineral. This dissolution generates connected secondary pore networks (Figure 18). These processes collectively

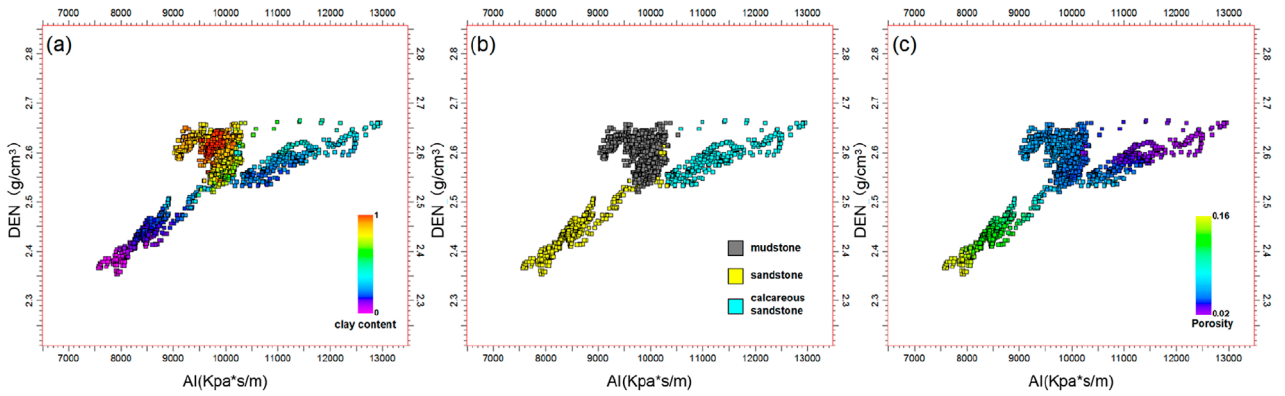

FIGURE 17
Distribution of Acoustic Impedance, Porosity, and Clay Content in Different Lithologies. **(a)** Relationship between clay content and acoustic impedance/density; **(b)** Relationship between lithology and acoustic impedance/density; **(c)** Relationship between porosity and acoustic impedance/density.

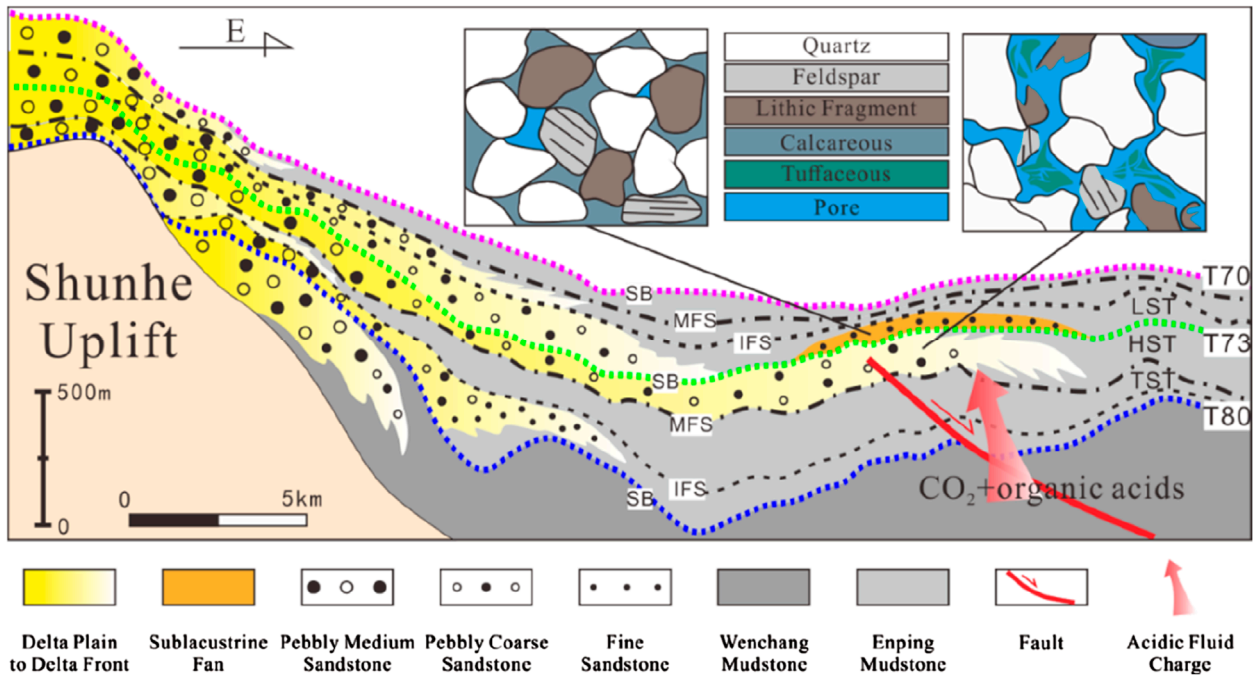

FIGURE 18
Developmental model of the Enping formation reservoirs.

counteract regional compaction effects, facilitating the development of moderate porosity-permeability reservoirs in tight backgrounds. This depositional-diagenetic coupling model defines the subaqueous distributary channel microfacies as a critical sweet spot for tight gas exploration in the Baiyun Sag.

6 Conclusion

In deep-water exploration areas with limited well control, seismic attribute techniques based on 90° phase rotation effectively identify and characterize the spatial distribution of sand bodies. By integrating paleogeomorphological reconstruction with insights into the source-to-sink system derived from seismic reflection characteristics, and by comparing the interpreted system with modern analogues, the planar distribution of sedimentary facies can be further deduced, providing critical support for reservoir prediction.

Seismic attribute slice analysis not only aids in recognizing the macroscopic distribution of sedimentary bodies but also serves as an indicator for qualitative to semi-quantitative assessment of reservoir quality. Building on the understanding of key controls on reservoir properties achieved through petrological and petrophysical analyses, and coupled with investigating the influence

of rock composition on acoustic impedance response, qualitative relationships between seismic attributes and reservoir parameters can be established. This approach enhances the application potential of seismic attributes in predicting reservoir quality. Under conditions of scarce drilling data, seismic sedimentology demonstrates significant value by advancing from morphological description to physical property characterization.

The Eocene Enping Formation was dominated by highstand braided deltas and lowstand sublacustrine fans, sourced from the Shunhe Uplift and shaped by regional tectonics and paleogeomorphology. The reservoir primarily comprise lithic arkose and litharenite with moderate compositional and textural maturity, exhibiting moderate-low porosity and low-ultralow permeability. Pore systems are dominated by dissolution features from tuffaceous matrix, feldspars, and rock fragments, though fine-microscale throats limit connectivity.

Reservoir quality is fundamentally controlled by the synergy between depositional and diagenetic processes. Coarse-grained, moderately sorted sandstones in braided delta front subaqueous distributary channels provide optimal framework for porosity preservation. Although compaction significantly degrades deep-buried reservoirs, dissolution enhances porosity during shallow burial via selective leaching of unstable components.

Exploration efforts should prioritize shallow-buried braided delta front subaqueous distributary channels, where favorable grain-size distributions and intense dissolution jointly enhance reservoir quality. These zones represent key targets for unlocking the Enping Formation's tight gas potential, offering a strategic pathway for future exploration in the Baiyun Sag.

Data availability statement

The original contributions presented in the study are included in the article/supplementary material, further inquiries can be directed to the corresponding author.

Author contributions

YZ: Writing – review and editing, Writing – original draft, Methodology, Conceptualization, Data curation. HS: Writing – review and editing, Data curation, Visualization. LX: Investigation, Methodology, Writing – review and editing, Supervision. HY: Data curation, Methodology, Supervision, Writing – review and editing. XW: Funding acquisition, Resources, Writing – review and editing. BC: Writing – review and editing, Methodology, Data curation.

Funding

The author(s) declare that financial support was received for the research and/or publication of this article. This study was supported by the self-initiated research project of CNOOC (China) Limited, Shenzhen Branch, "Study on Hydrocarbon Accumulation Process and Enrichment Patterns in the Middle-Deep Reservoirs of the Panyu 35-2 Structure" (Grant No. YXKY-ZL-SZ-2025-02). The funder was not involved in the study design, collection, analysis, interpretation of data, the writing of this article, or the decision to submit it for publication.

Conflict of interest

Authors YZ, HS, LX, HY, XW and BC were employed by Shenzhen Branch of China National Offshore Oil Corporation (CNOOC) Co., Ltd and CNOOC Deepwater Development.

Generative AI statement

The author(s) declare that no Generative AI was used in the creation of this manuscript.

Any alternative text (alt text) provided alongside figures in this article has been generated by Frontiers with the support of artificial intelligence and reasonable efforts have been made to ensure accuracy, including review by the authors wherever possible. If you identify any issues, please contact us.

Publisher's note

References

Beard, C. D., and Weyl, P. K. (1973). Influence of texture on porosity and permeability of unconsolidated sand. *AAPG Bull.* 57, 349–369. doi:10.1306/819A4272-16C5-11D7-8645000102C1865D

Chen, G. J., Du, G. C., Zhang, G. C., Lv, C. F., Wang, Q., and Chen, J. (2009). Diagenesis and main factors controlling the tertiary reservoir properties of the panyu low-uplift reservoirs, pearl river mouth basin. *Nat. Gas. Geosci.* 20 (06), 854–861.

Dahm, C. G., and Graebner, R. J. (1979). Field development with three-dimensional seismic methods in Gulf of Thailand-a case history. *Offshore Technol. Conf.* (Paper 3657), 2591–2595. doi:10.1071/EG979185

Deng, H. W., Wang, H. L., and Wang, D. Z. (2001). Control of Paleo-Morphology to stratigraphic sequence in continental rift basins: take lower tertiary if western slope in bozhong depression as an example. *Oil & Gas Geol.* (05), 53–56. doi:10.11743/ogg20010402

Ding, W. W., Li, M. B., He, M., Tang, Y., and Fang, Y. B. (2009). Cenozoic tectono-sedimentary evolution in the middle part of northern continental shelf-slope region, South China Sea. *Geol. J. China Univ.* 15 (03), 339–350.

Dong, C. M., Zhang, X. g., and Lin, C. Y. (2006). Discussions on several issues about seismic sedimentology. *Oil Geophys. Prospect.* 41 (4), 405–409. doi:10.3321/j.issn:1000-7210.2006.04.010

Dong, D. D., Wang, D. W., Zhang, G. C., Wu, S. G., and Yuan, S. Q. (2009). Cenozoic tectonic and sedimentary evolution of deepwater area, pearl river mouth basin. *J. China Univ. Petroleum Ed. Nat. Sci.* 33 (05), 17–22+29.

Galloway, W. E., and Hobday, D. K. (1983). *Terrigenous clastic depositional systems: applications to petroleum, coal, and uranium expliration*. New York: Springer-Verlag, 423.

Gao, Y. D., Lai, W. C., Zhang, X. T., and Zhang, J. W. (2024a). New progress and future directions of CNOOC oil and gas exploration. *China Offshore Oil Gas* 36 (3), 1–10. doi:10.11935/j.issn.1673-1506.2024.00.003

Gao, Y. D., Zhu, W. L., Peng, G. R., Long, Z. L., Wang, X. D., Shi, C., et al. (2024b). Evaluation of source rocks and prediction of oil and gas resources distribution in Baiyun Sag, Pearl river mouth basin, China. *Petroleum Explor. Dev.* 51 (05), 1138–1150. doi:10.1016/s1876-3804(25)60531-3

He, M., Zhu, W. L., Wu, Z., Zhon, G. F., Ren, J. Y., Liu, L. H., et al. (2019). Neotectonic movement characteristics and hydrocarbon accumulation of the pearl river mouth basin. *China Offshore Oil Gas* 31 (05), 9–20.

Jiang, L. Z., Gu, J. Y., and Guo, B. C. (2004). Characteristics and mechanism of low permeability clastic reservoir in Chinese petroliferous basin. *Acta Sedimentol. Sin.* (01), 13–18. doi:10.1109/JLT.2003.821766

Li, W. G., Zhang, X. P., and Zhong, Y. M. (2005). Formation mechanism of secondary dissolved pores in arcose. *Oil & Gas Geol.* (02), 220–223+229. doi:10.1016/j.molcatb.2005.02.001

Li, C. H., Wang, J. H., Liu, B. J., Su, A., Xu, D. H., Luo, Q. Y., et al. (2014). Types and distribution of the Paleogene sedimentary facies in baiyun depression of pearl river mouth basin. *Acta Sedimentol. Sin.* 32 (06), 1162–1170. doi:10.14027/j.cnki.cjxb.2014.06.018

Liao, J. H., Wu, K. Q., and Er, C. (2022). Deep reservoir characteristics and effective reservoir control factors in Baiyun Sag of Pearl River Mouth Basin. *Earth Sci.* 47 (07), 2454–2467. doi:10.3799/dqkx.2022.017

Lindsey, J. P. (1989). The Fresnel zone and its interpetive significance. *Lead. Edge* 8 (10), 33–39. doi:10.1190/1.1439575

Liu, B. J., Pang, X., Yan, C. Z., Liu, J., Lian, S. Y., He, M., et al. (2011a). Evolution of the Oligocene-Miocene shelf slope-break zone in the Baiyun deep-water area of the Pearl River Mouth Basin and its significance in oil-gas exploration. *Acta Pet. Sin.* 32 (02), 234–242. doi:10.1007/s12182-011-0123-3

Liu, B. J., Pang, X., Yan, C. Z., Lian, S. Y., Liu, J., He, M., et al. (2011b). An analysis of depositional evolution and its controls in Baiyun deep-water area, Pearl River Mouth Basin. *China Offshore Oil Gas* 23 (01), 19–25. doi:10.3969/j.issn.1673-1506.2011.01.004

Liu, B. J., Pang, X., Xie, S. W., Mei, L. F., Zheng, J. Y., Sun, H., et al. (2022). Control effect of crust-mantle detachment fault activity on deep large Delta sedimentary System in Baiyun Sag, Pearl River mouth Basin. *Earth Sci.* 47 (07), 2354–2373. doi:10.3799/dqkx.2022.035

Liu, J., Peng, G. R., Zhang, L. L., Li, H. B., Wang, X. D., Wu, Z., et al. (2025). Genesis and types of buried hills in the tectonic setting of the inheriting continental margin in Baiyun Sag, Northern South China Sea. *Earth Sci.* 50 (02), 405–418. doi:10.3799/dqkx.2023.187

Ma, M., Chen, G. J., Lv, C. F., Zhang, G. C., Li, C., Zhao, Z., et al. (2016). Eocene-low Oligocene sedimentary environment and mudstone provenance in baiyun sag, pearl river mouth basin. *Acta Pet. Sin.* 37 (05), 610–621. doi:10.7623/syxb201605005

Ma, Y. K., Xu, L. Y., Sun, H., Wang, X. M., Li, X. Y., and Zhou, F. J. (2024). Diagenetic characteristics of reservoirs and middle-deep reservoirs exploration potential in Baiyun Sag, Pearl River mouth Basin. *J. Jilin Univ. Earth Sci. Ed.* 54 (06), 1940–1950. doi:10.13278/j.cnki.j.juese.20240240

Mi, L. J., Zhang, G. C., Fu, N., He, Q., and Ma, L. W. (2006). An analysis of hydrocarbon source and accumulation in Panyu low-uplift and north slope of Baiyun Sag, Pearl River Mouth Basin. *China Offshore Oil Gas* (03), 161–168. doi:10.3969/j.issn.1673-1506.2006.03.003

Mi, L. J., Liu, B. J., He, M., Pang, X., and Liu, J. (2016). Petroleum geology characteristics and exploration direction in Baiyun deep water area, northern continental margin of the South China Sea. *China Offshore Oil Gas* 28 (02), 10–22. doi:10.11935/j.issn.1673-1506.2016.02.002

Mi, L. J., Zhang, G. C., Shen, H. L., Liu, Z., Guo, R., Zhong, K., et al. (2018). Eocene-Lower Oligocene sedimentation characteristics of Baiyun Sag in the deep water area of Pearl River Mouth Basin. *Acta Pet. Sin.* (01), 29–34. doi:10.3321/j.issn:0253-2697.2008.01.005

Mitchum, R. M., Vail, P. R., and Thompson, S. (1977). "Seismic stratigraphy and global changes of sea level, part 2: the depositional sequence as a basic unit for stratigraphic analysis,". *Seismic stratigraphy: applications to hydrocarbon exploration*. Editor C. E. Payton (American Association of Petroleum Geologists), 26, 53–62.

Pang, X., Chen, C. M., Peng, D. J., Zhou, D., Shaco, L., He, M., et al. (2008). Basic geology of Baiyun deep-water area in the northern South China Sea. *China Offshore Oil Gas* (04), 215–222.

Pang, J. G., Yang, Y. Y., Li, W. H., Li, L., and Wen, Y. (2013). Study development of palaeogeomorphology reconstructions in continental facies hydrocarbon basin. *J. Xi'an Univ. Sci. Technol.* 33 (04), 424–430. doi:10.3969/j.issn.1672-9315.2013.04.009

Pang, X., Ren, J. Y., Zheng, J. Y., Liu, J., Yu, P., and Liu, B. J. (2018). Petroleum geology controlled by extensive detachment thinning of continental margin crust: a case study of Baiyun sag in the deep-water area of northern South China Sea. *Petroleum Explor. Dev.* 45 (01), 29–42. doi:10.1016/s1876-3804(18)30003-x

Shi, H. S., Liu, B. J., Yan, C. Z., Zhu, M., Pang, X., Qin, C. G., et al. (2010). Hydrocarbon accumulation conditions and exploration potential in Baiyun-Liwan deepwater area, Pearl river Mouth Basin. *China Offshore Oil Gas* 22 (06), 369–374. doi:10.3969/j.issn.1673-1506.2010.06.003

Vail, P. R., Mitchum, R. M., and Thompson, S. (1977). "Seismic stratigraphy and global changes of sea level, part 3: relative changes of sea level from coastal onlap,". *Seismic stratigraphy: applications to hydrocarbon exploration*. Editor C. W. Payton (American Association of Petroleum Geologists), 26, 63–81.

Wang, Z. H., Jiang, N. C., and Lv, Q. B. (2008). Concepts, methodologies, and applications of seismic sedimentology. *Jianghan Petroleum Sci. Technol.* 18 (2), 7–11. doi:10.19406/j.cnki.cqkjxyxbzkb.2008.03.009

Wang, J. H., Peng, G. R., Liu, B. J., Zheng, J. Y., and Yang, F. (2019). Flattening diagenesis of clastic rocks and quantitative characterization of sedimentary control on reservoir properties: a case study of Baiyun Sag in Pearl River Mouth Basin. *Acta Pet. Sin.* 40 (S1), 115–123. doi:10.7623/syxb2019S1010

Wang, X., Gao, J. H., Pang, Y. D., Wu, H. H., Yu, Q., Zhang, H. B., et al. (2024). Reservoir characteristics and controlling factors of Jurassic Yan 10 Member sandy braided river of M34 Block, Ordos Basin. *J. Northeast Petroleum Univ.* 48 (03), 23–39. doi:10.3969/j.issn.2095-4107.2024.02.003

Wen, J., Zhao, J. Z., Li, J., and Er, C. (2022). Characteristics of mid-deep Paleogene sandstone reservoirs in Baiyun Sag and controlling effect of dissolution on high-quality reservoirs. *Special Oil & Gas Reservoirs* 29 (06), 47–55. doi:10.3969/j.issn.1006-6535.2022.06.006

Xiang, X. H., Zhang, L. L., Lu, Y., Qiao, P. J., Chen, S. H., Wu, M. S., et al. (2024). Paleogene sediment source evolution and palaeogeographic significance in deep-water area of the northern South China Sea. *J. Palaeogeogr.* 26 (02), 296–307. doi:10.7605/gdlxb.2024.02.014

Xie, S. W., Liu, B. J., Pang, X., Ding, L., Wu, Y. X., Liu, D. Q., et al. (2023). Sedimentary environment evolution and hydrocarbon control in Baiyun Sag of Pearl River Mouth Basin during rifting period. *Nat. Gas. Geosci.* 34 (02), 296–311. doi:10.11764/j.issn.1672-1926.2022.09.003

Xu, C. G., Lai, W. C., Xue, Y. A., Yu, S., and Cheng, J. C. (2004). Palaeo-geomorphology analysis for the Paleogene reservoir prediction in Bohai sea area. *Petroleum Explor. Dev.* (05), 53–56. doi:10.0000/1000-0747-31-913

Yang, X. P., Zhao, W. Z., Zhou, C. N., Chen, M. J., and Guo, Y. R. (2007). Origin of low-permeability reservoir and distribution of favorable reservoir. *Acta Pet. Sin.* (04), 57–61. doi:10.1016/S1872-5813(07)60034-6

Zeng, H. L., Backus, M. M., Barrow, K. T., and Noel, T. (1998a). Stratal slicing, part I: realistic 3-D seismic model. *Geophysics* 63 (2), 502–513. doi:10.1190/1.1444351

Zeng, H. L., Henry, S. C., and Riola, J. P. (1998b). Stratal slicing, part II: real 3-D seismic data. *Geophysics* 63 (2), 514–522. doi:10.1190/1.1444352

Zhang, G. C. (2010). Tectonic evolution of deepwater area of northern continental margin in South China Sea. *Acta Pet. Sin.* 31 (04), 528–533+541. doi:10.1016/S1876-3804(11)60008-6

Zhang, J. H., Zhou, Z. X., Tan, M. Y., Feng, D. Y., Gao, R. T., Zhong, L., et al. (2007). Discussions on several issues in seismic slice interpretation. *Oil Geophys. Prospect.* 42 (3), 348–352. doi:10.3321/j.issn:1000-7210.2007.03.022

Zhang, G. C., Yang, H. C., Chen, Y., Ji, M., Wang, K., Yang, D. S., et al. (2014). The Baiyun Sag: a giant rich gas-generation sag in the deepwater area of the Pearl River Mouth Basin. *Nat. Gas. Ind.* 34 (11), 11–25. doi:10.3787/j.issn.1000-0976.2014.11.002

Zhang, X. T., Peng, G. R., Xie, S. W., Wei, Z., Shan, X. L., He, W. T., et al. (2024). Characteristics of reservoir diagenesis in the Zhuhai formation in the southwestern Baiyun depression, Pearl River Mouth Basin, and its influence on reservoir physical properties. *Nat. Gas. Geosci.* 35 (03), 379–392. doi:10.11764/j.issn.1672-1926.2023.11.009

Zhang, X. T., Chen, C., Xiang, X. H., Huang, Y. P., Huang, W. Y., and Cao, Y. H. (2025). Characteristics, distribution patterns, and resource potential of source rocks in Eocene of Baiyun Sag. *China Offshore Oil Gas* 37 (03), 56–67. doi:10.11935/j.issn.1673-1506.2025.03.005

Zhou, C. N., Tao, S. Z., Zhou, H., Zhang, X. X., He, D. B., Zhou, C. M., et al. (2008). Genesis, classification and evaluation method of diagenetic facies. *Petroleum Explor. Dev.* 35 (05), 526–540. doi:10.1016/s1876-3804(09)60086-0

Zhu, X. M., Dong, Y. L., Hu, Y. H., Luo, Q., Wang, M., Yang, D. Q., et al. (2011). Seismic sedimentology study of fine sequence stratigraphic framework:a case study of the Hetaoyuan Formation in the Biyang Sag. *Oil & Gas Geol.* 32 (5), 615–624. doi:10.11743/ogg20110416

Zhu, J. Z., Shi, H. S., Pang, X., Zhang, Z. L., Liu, B. J., Long, Z. L., et al. (2012). Origins and accumulation characteristics of hydrocarbons in eastern Baiyun deepwater area. *China Pet. Explor.* 17 (04), 20–28+6. doi:10.3969/j.issn.1672-7703.2012.04.004